PHILOSOPHICAL TRANSACTIONS OF THE ROYAL SOCIETY A

Phil. Trans. R. Soc. A (2006) **364**, 1135–1154
doi:10.1098/rsta.2006.1759
Published online 21 March 2006

A mathematical model of pacemaker activity recorded from mouse small intestine

By Jae Boum Youm[1], Nari Kim[1], Jin Han[1], Euiyong Kim[1], Hyun Joo[1], Chae Hun Leem[2], Gazunori Goto[3], Akinori Noma[3] and Yung E. Earm[4,*]

[1]*Mitochondrial Signaling Laboratory, Department of Physiology and Biophysics, College of Medicine, 2020 Cardiovascular Institute, Inje University, Busan 614-735, South Korea*
[2]*Department of Physiology, University of Ulsan College of Medicine, 388-1 Poongnap-Dong Songpa-Ku, Seoul 138-736, South Korea*
[3]*Department of Physiology, Faculty of Medicine, Kyoto University, Yoshida-Konoe, Sakyo-ku, Kyoto 606-8501, Japan*
[4]*Department of Physiology and National Research Laboratory for Cellular Signalling, Seoul National University College of Medicine, 28 Yonkeun-Dong, Chongno-Ku 110-799, Seoul, South Korea*

The pacemaker activity of interstitial cells of Cajal (ICCs) has been known to initiate the propagation of slow waves along the whole gastrointestinal tract through spontaneous and repetitive generation of action potentials. We studied the mechanism of the pacemaker activity of ICCs in the mouse small intestine and tested it using a mathematical model. The model includes ion channels, exchanger, pumps and intracellular machinery for Ca^{2+} regulation. The model also incorporates inositol 1,4,5-triphosphate (IP_3) production and IP_3-mediated Ca^{2+} release activities. Most of the parameters were obtained from the literature and were modified to fit the experimental results of ICCs from mouse small intestine. We were then able to compose a mathematical model that simulates the pacemaker activity of ICCs. The model generates pacemaker potentials regularly and repetitively as long as the simulation continues. The frequency was set at 20 min^{-1} and the duration at 50% repolarization was 639 ms. The resting and overshoot potentials were −78 and +1.2 mV, respectively. The reconstructed pacemaker potentials closely matched those obtained from animal experiments. The model supports the idea that cyclic changes in $[Ca^{2+}]_i$ and $[IP_3]$ play key roles in the generation of ICC pacemaker activity in the mouse small intestine.

Keywords: Cajal cell; pacemaker; small intestine; simulation

1. Introduction

Rhythmical contractions of the gastrointestinal (GI) tract are associated with the pacemaker electrical activity generated in the muscle layers, which occurs at

* Author for correspondence (earmye@snu.ac.kr).

One contribution of 13 to a Theme Issue ‘Biomathematical modelling I’.

low frequency in the absence of an extrinsic nervous stimulation. The ICCs, distributed in the myenteric region of the GI wall, have been suggested to initiate the pacemaker activity (Tomita 1981), which then propagates to the smooth muscle cells through gap junctions to generate the contraction of the whole GI tract (Dickens *et al.* 1999). This pacemaker activity is represented by the driving potential or pacemaker potential of ICC. However, the mechanism of the pacemaker activity is not yet well understood.

Recently, Goto *et al.* (2004) recorded the pacemaker activity in a single ICC prepared from mouse small intestine. The amplitude of the pacemaker potential was slightly above 70 mV and a series of voltage-clamp experiments was performed to investigate the mechanism of the pacemaker activity. They recorded a large inward current with an autonomous time course (I_{AI}) by applying a depolarizing pulse and concluded that the spontaneous depolarization is caused by the activation of the I_{AI}. Now, it is possible to develop a mathematical model to explain the regenerative nature of pacemaker potentials in a single ICC. Although some investigators have made mathematical models to simulate the regenerative potentials in the GI tract (Miftakhov *et al.* 1999; Edwards & Hirst 2003, 2005), the models are still phenomenological in the point of method or approach, and they focused on the electrical activity of a larger cellular network rather than a single ICC.

In this study, pacemaker potentials of ICCs from the mouse small intestine were simulated with a mathematical model to explain the regenerative nature of the pacemaker potentials and the underlying $[Ca^{2+}]_i$ changes. The model faithfully reproduces the pacemaker activity and suggests a possible mechanism.

2. Methods

Modelling of the pacemaker activity in the ICCs is still at a very early stage in comparison with modelling of the pacemaker activity of the heart. Furthermore, the experimental results describing the Ca^{2+} dynamics, ion channels and intracellular metabolic pathways in ICCs are scarce. Thus, although our object is to make a simulation model of mouse ICCs, the equations and parameters used were partly derived from the heart models (Luo & Rudy 1994; Matsuoka *et al.* 2003) and were modified to reproduce the pacemaker activity of mouse ICCs (table 1).

(*a*) *Cellular geometry*

The ICCs isolated from mouse small intestine have a spindle-shaped cell body with extending processes. The cell body is 5–15 μm wide, and the measured mean capacitance is 21–25 pF (Kim *et al.* 2002; Koh *et al.* 2002; Goto *et al.* 2004). The cell volume is simply calculated from a cell capacitance of 25 pF by assuming that the cell has the same hexahedral geometry as guinea-pig ventricular myocytes ($100\times20\times8\ \mu m^3$) except for its smaller scale in cell dimension (see Matsuoka *et al.* 2003). Given the surface area provided by the capacitance and the hexahedral geometry, the cell dimension was determined and used to calculate the cell volume. The V_i for ion diffusion was assumed to be 50% of the cell volume (Matsuoka *et al.* 2003). We also divided the SR into a Ca^{2+}-release

Table 1. Abbreviations and symbols.

ICCs	interstitial cells of Cajal
SR	sarcoplasmic reticulum
C_{m}	membrane capacitance, pF
V	membrane potential, mV
V_{i}	cell volume accessible for ion diffusion, $\mu\mathrm{m}^3$
V_{up}	volume of SR uptake site, $\mu\mathrm{m}^3$
V_{rel}	volume of SR release site, $\mu\mathrm{m}^3$
$I_{\mathrm{a}}\mathrm{X}$	ion X component of current I_{a}, pA
$I_{\mathrm{net}}\mathrm{X}$	whole cell current carried by ion X, pA
I_{ext}	current applied through the electrode, pA
I_{tot}	total current of ion channels, exchanger and pumps, pA
X_{CF}	constant field equation for ion X, mM
E_{X}	equilibrium potential for ion X, mV
F	Faraday constant, 96.4867 C mmol^{-1}
R	gas constant, 8.3143 C mVK^{-1} mmol^{-1}
T	absolute temperature, K
z_{X}	valence of ion X
$[\mathrm{X}^z]_{\mathrm{i}}$	intracellular concentration of ion X, mM
$[\mathrm{X}^z]_{\mathrm{o}}$	extracellular concentration of ion X, mM
$[\mathrm{X}]_{\mathrm{f}}$	concentration of X in the free form, mM
$[\mathrm{X}]_{\mathrm{total}}$	concentration of X in the free and bound form, mM
$[\mathrm{Ca}]_{\mathrm{i}}$	total cytosolic calcium concentration in the free and bound form, mM
$[\mathrm{Ca}]_{\mathrm{rel}}$	total calcium concentration in the free and bound form in the release pool of SR, mM
TRPN	troponin
CMDN	calmodulin
CSQN	calsequestrin
PIP_2	phosphatidyl-1,4-bisphosphate
IP_3	inositol 1,4,5-triphosphate
IP_4	inositol 1,3,4,5-tetraphosphate
$\mathrm{IP}_3\mathrm{R}$	inositol 1,4,5-triphosphate receptor channel
Km_{X}	Michaelis constant for ion X binding
C, O, I, B	closed, open, inactivated and blocked state, respectively
p_{o}	open probability of a channel
m, h	activation and inactivation gate, respectively
α_m, β_m	opening and closing rate constants, respectively, of m, ms^{-1}
α_h, β_h	opening and closing rate constants, respectively, of h, ms^{-1}

site in the junctional space and a Ca^{2+}-uptake site in the deep cytoplasmic space (Mackenzie *et al.* 2001). The cell capacitance and the volume of each compartment are summarized in table 2.

(*b*) *Ca^{2+}-binding proteins*

The amounts of Ca^{2+} that bound to troponin, calmodulin and calsequestrin were estimated using the approach described by Luo & Rudy (1994). We assumed that the rates of Ca^{2+} binding are so fast that the concentration of free calcium gets equilibrium with the Ca^{2+}-binding proteins instantaneously. The concentrations of free calcium and Ca^{2+}-binding proteins satisfy the following

Table 2. Cell geometry.

parameter	value
C_{m}	25 pF
V_{i}	715.5 μm^3
V_{up}	$0.1\,V_{\mathrm{i}}$
V_{rel}	$0.01\,V_{\mathrm{i}}$

Table 3. Ca^{2+}-binding proteins.

parameter	value
Km_{TRPN}	0.0005 mM
Km_{CMDN}	0.00238 mM
Km_{CSQN}	0.8 mM

equations at equilibrium (table 3):

$$[\mathrm{Ca}^{2+}]_{\mathrm{i}} = \frac{[\mathrm{Ca}]_{\mathrm{i}}}{1 + ([\mathrm{TRPN}]_{\mathrm{f}}/Km_{\mathrm{TRPN}}) + ([\mathrm{CMDN}]_{\mathrm{f}}/Km_{\mathrm{CMDN}})}, \tag{2.1}$$

$$[\mathrm{TRPN}]_{\mathrm{f}} = \frac{[\mathrm{TRPN}]_{\mathrm{total}}}{1 + ([\mathrm{Ca}^{2+}]_{\mathrm{f}}/Km_{\mathrm{TRPN}})}, \tag{2.2}$$

$$[\mathrm{CMDN}]_{\mathrm{f}} = \frac{[\mathrm{CMDN}]_{\mathrm{total}}}{1 + ([\mathrm{Ca}^{2+}]_{\mathrm{f}}/Km_{\mathrm{CMDN}})}, \tag{2.3}$$

$$[\mathrm{Ca}^{2+}]_{\mathrm{rel}} = \frac{[\mathrm{Ca}]_{\mathrm{rel}}}{1 + ([\mathrm{CSQN}]_{\mathrm{f}}/Km_{\mathrm{CSQN}})}, \tag{2.4}$$

$$[\mathrm{CSQN}]_{\mathrm{f}} = \frac{[\mathrm{CSQN}]_{\mathrm{total}}}{1 + ([\mathrm{Ca}^{2+}]_{\mathrm{rel}}/Km_{\mathrm{CSQN}})}. \tag{2.5}$$

(*c*) *Calculation of the membrane potential and internal ion concentrations*

(i) *Membrane potential*

Time-dependent changes in the membrane potential are described by the following equation:

$$\mathrm{d}V/\mathrm{d}t = -(I_{\mathrm{tot}} + I_{\mathrm{ext}})/C_{\mathrm{m}}, \tag{2.6}$$

where I_{ext} is the current applied through the electrode by the current clamp or whole-cell voltage-clamp circuitry. I_{tot} includes an inward rectifier K^+ current (I_{K1}), an L-type Ca^{2+} current (I_{CaL}), a voltage-dependent and dihydropyridine

(DHP)-resistant current (I_{VDDR}), an autonomous inward current (I_{AI}), a Na^+/Ca^{2+} exchange current (I_{NaCa}), a Na^+/K^+ pump current (I_{NaK}) and a plasmalemmal Ca^{2+} pump current (I_{PMCA}):

$$I_{\mathrm{tot}} = I_{\mathrm{K1}} + I_{\mathrm{CaL}} + I_{\mathrm{VDDR}} + I_{\mathrm{AI}} + I_{\mathrm{NaCa}} + I_{\mathrm{NaK}} + I_{\mathrm{PMCA}}. \tag{2.7}$$

(ii) *Internal ion concentration*

The cytosolic ionic concentrations were determined by the net ion fluxes across the plasma and SR membranes. The net ion fluxes were separated into three ionic components (Na^+, K^+ and Ca^{2+}) based on the ionic selectivity of each ion channels, exchanger and pumps. The ionic component of each channel current is described by the constant field equation (see equation (2.14)).

$$\mathrm{d}[\mathrm{Na}^+]_{\mathrm{i}}/\mathrm{d}t = -I_{\mathrm{net}}\mathrm{Na}/(z_{\mathrm{Na}}FV_{\mathrm{i}}), \tag{2.8}$$

$$\mathrm{d}[\mathrm{K}^+]_{\mathrm{i}}/\mathrm{d}t = -I_{\mathrm{net}}\mathrm{K}/(z_{\mathrm{K}}FV_{\mathrm{i}}), \tag{2.9}$$

$$\mathrm{d}[\mathrm{Ca}^{2+}]_{\mathrm{i}}/\mathrm{d}t = -(I_{\mathrm{net}}\mathrm{Ca} - I_{\mathrm{IP3R}} + I_{\mathrm{up}} - I_{\mathrm{leak}})/(z_{\mathrm{Ca}}FV_{\mathrm{i}}), \tag{2.10}$$

$$I_{\mathrm{net}}\mathrm{Na} = I_{\mathrm{CaL}}\mathrm{Na} + I_{\mathrm{AI}}\mathrm{Na} + 3I_{\mathrm{NaK}} + 3I_{\mathrm{NaCa}}, \tag{2.11}$$

$$I_{\mathrm{net}}\mathrm{K} = I_{\mathrm{K1}} + I_{\mathrm{CaL}}\mathrm{K} + I_{\mathrm{AI}}\mathrm{K} - 2I_{\mathrm{NaK}}, \tag{2.12}$$

$$I_{\mathrm{net}}\mathrm{Ca} = I_{\mathrm{CaL}}\mathrm{Ca} + I_{\mathrm{VDDR}} + I_{\mathrm{AI}}\mathrm{Ca} - 2I_{\mathrm{NaCa}} + I_{\mathrm{PMCA}}, \tag{2.13}$$

$$\mathrm{X}_{\mathrm{CF}} = \frac{z_{\mathrm{X}}FV}{RT}\,\frac{[\mathrm{X}^{z_{\mathrm{X}}}]_{\mathrm{i}} - [\mathrm{X}^{z_{\mathrm{X}}}]_{\mathrm{o}}\exp\left(\frac{-z_{\mathrm{X}}FV}{RT}\right)}{1-\exp\left(\frac{-z_{\mathrm{X}}FV}{RT}\right)}. \tag{2.14}$$

(*d*) *Ion channels*

(i) *Inward rectifier K^+ current (I_{K1})*

The I_{K1} has been reported in cultured ICCs from the mouse small intestine (Koh *et al.* 1998). The I_{K1} is thought to repolarize the pacemaker potential. We adopted the Kyoto model (Matsuoka *et al.* 2003) and modified it to reproduce the pacemaker activity of ICCs, as described below (table 4):

State C goes into state O reversibly,

$$\mathrm{C} \underset{\beta_n}{\overset{\alpha_n}{\rightleftarrows}} \mathrm{O}.$$

State O also goes into state B reversibly,

$$\mathrm{O} \underset{\lambda}{\overset{\mu}{\rightleftarrows}} \mathrm{B}.$$

Table 4. Ion channels.

I_{K1}	G_{K1}: channel conductance when $[K^+]_i$ is 5.4 mM, 4.32 pA mV^{-1} n: activation gate α_n, β_n: opening and closing rate constants, respectively, of n, ms^{-1} f_B, f_U: fraction of block and unblock, respectively μ, λ: block and unblock rate constants, respectively, ms^{-1}
I_{CaL}	P_{CaL}: conversion factor, 57.6
I_{VDDR}	P_{VDDR}: conversion factor, 15.84
I_{AI}	P_{AI}: conversion factor, 15.61 Km_{Cai}: 0.003 mM

We assumed the transition between state O and B occurs instantaneously.

$$I_{K1} = G_{K1}([K^+]_o/5.4)^{0.62}(V - E_K)nf_U, \tag{2.15}$$

$$\frac{\alpha_n}{\alpha_n + \beta_n} = \frac{1}{1 + 0.1\exp((V - E_K)/15) + 0.048\exp((V - E_K)/7)}, \tag{2.16}$$

$$\alpha_n + \beta_n = \frac{2.5}{4.7\exp((V - E_K)/28.7)} + \frac{2.5}{6.0\exp((V - E_K)/25.8)}, \tag{2.17}$$

$$\mu = 3.3\exp((V - E_K - 6)/15), \tag{2.18}$$

$$\lambda = 26\exp((E_K - V - 6)/52), \tag{2.19}$$

$$f_B = \frac{\mu}{\mu + \lambda}, \tag{2.20}$$

$$f_U = \frac{\lambda}{\mu + \lambda}. \tag{2.21}$$

(ii) *L-type Ca^{2+} current (I_{CaL})*

The depolarization of an ICC is thought to activate the I_{CaL} in the neighbouring ICC (Kim *et al.* 2002). The presence of an L-type Ca^{2+} channel was clearly demonstrated by Cho & Daniel (2005) using the double-immunofluorescence labelling method. We adopted the classical two-state model and used the rate constants obtained from the voltage-clamp data of Kim *et al.* (2002). In addition, we added the Ca^{2+}-dependent inactivation kinetics based on the Kyoto model (Matsuoka *et al.* 2003).

$$I_{CaL} = I_{CaL}Ca + I_{CaL}K + I_{CaL}Na, \tag{2.22}$$

$$I_{CaL}Ca = P_{CaL}Ca_{CF}mh, \tag{2.23}$$

$$I_{CaL}K = 0.001P_{CaL}K_{CF}mh, \tag{2.24}$$

$$I_{\mathrm{CaL}}\mathrm{Na} = 0.00005 P_{\mathrm{CaL}}\mathrm{Na}_{\mathrm{CF}} mh, \tag{2.25}$$

$$\alpha_m = 0.002175 \frac{V+30}{1-\exp((V+30)/(-2.5))}, \tag{2.26}$$

$$\beta_m = 0.0006315 \frac{V}{\exp(V/2.5)-1}, \tag{2.27}$$

$$\alpha_h = 1.775 \times 10^{-6} \frac{V+34}{\exp((V+34)/5.633)-1}, \tag{2.28}$$

$$\beta_h = 0.427[\mathrm{Ca}^{2+}]_{\mathrm{i}} \frac{V+64}{\exp((V+44)/(-4.16))+1}. \tag{2.29}$$

(iii) *Voltage-dependent and DHP-resistant current (I_{VDDR})*

The I_{VDDR} is thought to contribute to slow wave propagation in the GI tract. The I_{VDDR} was fully studied and described by Kim *et al.* (2002) in the ICCs isolated from mouse colon and small intestine. We used the parameter values obtained from their results to reconstruct the I_{VDDR}:

$$I_{\mathrm{VDDR}} = P_{\mathrm{VDDR}}\mathrm{Ca}_{\mathrm{CF}} mh, \tag{2.30}$$

$$\frac{\alpha_m}{\alpha_m+\beta_m} = \frac{1}{1+\exp((V+26)/(-6))}, \tag{2.31}$$

$$\frac{1}{\alpha_m+\beta_m} = 0.6 + \frac{5.4}{1+\exp(0.03(V+100))}, \tag{2.32}$$

$$\frac{\alpha_h}{\alpha_h+\beta_h} = \frac{1}{1+\exp((V+66)/6)}, \tag{2.33}$$

$$\frac{1}{\alpha_h+\beta_h} = 10 + \frac{400}{1+\exp(0.02(V+65))}. \tag{2.34}$$

(iv) *Autonomous inward current (I_{AI})*

Goto *et al.* (2004) identified a large transient inward current evoked by depolarization under voltage-clamp conditions (see figure 1). They named the current as the autonomous inward current (I_{AI}) in that it shows an inward current with an autonomous time course by depolarizing clamp pulses. After I_{AI} was triggered, it took a regenerative time course and lasted about 500 ms. The reversal potential was around +3 mV suggesting that I_{AI} is a non-selective cation current. These authors proposed the I_{AI} as the pacemaker current generating the spontaneous depolarization of ICCs without an electrical

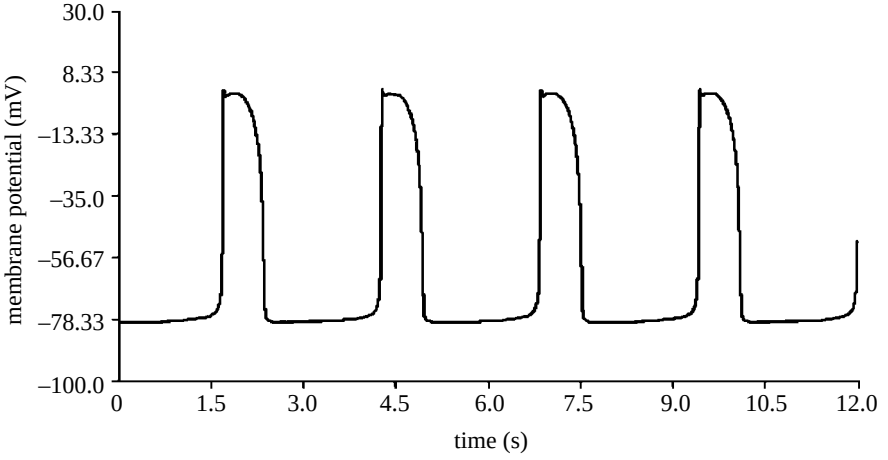

Figure 1. Reconstruction of pacemaker potentials in the ICCs from mouse small intestine. The simulation model fires regularly at a frequency of 20 min^{-1}. The diastolic time-interval between two successive pacemaker potentials (from 90% repolarization of the previous pacemaker potential to 10% depolarization of the next pacemaker potential) was approximately 1840 ms. This pacemaker activity was so stable that there was no significant changes in the electrical property after running the simulation for a period corresponding to 10 min on a cellular time-scale.

stimulus. We added a $[Ca^{2+}]_i$-dependent activation (see equation (2.39)) to reproduce a current with an autonomous time course.

$$I_{AI} = I_{AI}Ca + I_{AI}K + I_{AI}Na, \tag{2.35}$$

$$I_{AI}Ca = P_{AI}Ca_{CF}p_o, \tag{2.36}$$

$$I_{AI}K = 0.36P_{AI}K_{CF}p_o, \tag{2.37}$$

$$I_{AI}Na = 0.4P_{AI}Na_{CF}p_o, \tag{2.38}$$

$$p_o = 0.0017 + \frac{(1-0.0017)}{1 + (Km_{Cai}/[Ca^{2+}]_i)}. \tag{2.39}$$

(e) *Exchanger and pumps*

(i) *Na^+/Ca^{2+} exchange current (I_{NaCa})*

The kinetic model and scheme are basically identical to those of the Kyoto model (Matsuoka *et al.* 2003). The six-state model of Na^+/Ca^{2+} exchange was lumped into a two-state model according to Powell *et al.* (1993). The Michaelis constant (Km) and conversion factor (P_{NaCa}) were adjusted empirically to reproduce the repetitive and stable firing of pacemaker potentials (see figure 1; table 5)

$$\begin{array}{lll} E_2\mathrm{Na} \xleftrightarrow{Km_{Nao}} E_2 \xleftrightarrow{Km_{Cao}} E_2\mathrm{Ca} & & (1-y) \\ k_1 \uparrow\downarrow k_2 \qquad\qquad\qquad k_3 \uparrow\downarrow k_4 & & \beta_y \uparrow\downarrow \alpha_y \\ E_1\mathrm{Na} \xleftrightarrow{Km_{Nai}} E_1 \xleftrightarrow{Km_{Cai}} E_1\mathrm{Ca} & & y \end{array}$$

Table 5. Exchanger and pumps.

I_{NaCa}	P_{NaCa}: conversion factor, 8.458 Km_{Cai}: 0.00138 mM Km_{Cao}: 1.38 mM Km_{Nai}: 670 mM Km_{Nao}: 670 000 mM p(X): probability of state X y: gate in the reduced two-state model α_y, β_y: forward and backward rate constants, respectively, of y, ms^{-1}
I_{NaK}	P_{NaK}: conversion factor, 39.5 Km_{Nai}: 11 mM Km_{Ko}: 0.27 mM
I_{PMCA}	P_{PMCA}: conversion factor, 927.4 Km_{Cai}: 0.008 mM

$$I_{\mathrm{NaCa}} = P_{\mathrm{NaCa}}(k_1 p(E_1\mathrm{Na})y - k_2 p(E_2\mathrm{Na})(1-y)), \tag{2.40}$$

$$k_1 = \exp(0.32FV/(RT)), \tag{2.41}$$

$$k_2 = \exp((0.32-1)FV/(RT)), \tag{2.42}$$

$$k_3 = 1, \tag{2.43}$$

$$k_4 = 1, \tag{2.44}$$

$$p(E_1\mathrm{Na}) = \frac{1}{1+((1+[\mathrm{Ca}^{2+}]_{\mathrm{i}}/Km_{\mathrm{Cai}})/([\mathrm{Na}^{+}]_{\mathrm{i}}^{3}/Km_{\mathrm{Nai}}))}, \tag{2.45}$$

$$p(E_2\mathrm{Na}) = \frac{1}{1+((1+[\mathrm{Ca}^{2+}]_{\mathrm{i}}/Km_{\mathrm{Cao}})/([\mathrm{Na}^{+}]_{\mathrm{o}}^{3}/Km_{\mathrm{Nao}}))}, \tag{2.46}$$

$$p(E_1\mathrm{Ca}) = \frac{1}{1+((1+[\mathrm{Na}^{+}]_{\mathrm{i}}^{3}/Km_{\mathrm{Nai}})/([\mathrm{Ca}^{2+}]_{\mathrm{i}}/Km_{\mathrm{Cai}}))}, \tag{2.47}$$

$$p(E_2\mathrm{Ca}) = \frac{1}{1+((1+[\mathrm{Na}^{+}]_{\mathrm{o}}^{3}/Km_{\mathrm{Nao}})/([\mathrm{Ca}^{2+}]_{\mathrm{o}}/Km_{\mathrm{Cao}}))}, \tag{2.48}$$

$$\alpha_y = k_2 p(E_2\mathrm{Na}) + k_4 p(E_2\mathrm{Ca}), \tag{2.49}$$

$$\beta_y = k_1 p(E_1\mathrm{Na}) + k_3 p(E_1\mathrm{Ca}). \tag{2.50}$$

(ii) *Na^+/K^+ pump current (I_{NaK})*

Electrogenic $\mathrm{Na}^+/\mathrm{K}^+$ pump extrudes three Na^+ ions in exchange for two K^+ ions generating a net outward current. As the kinetics of the $\mathrm{Na}^+/\mathrm{K}^+$ pump have not been studied well in ICCs, we employed the model of Sakai *et al.* (1996)

obtained from rabbit sino-atrial node cells. The P_{NaK} was adjusted to maintain the $[Na^+]_i$ below 20 mM against the large Na^+ influx by I_{AI} during the depolarizing phase of a pacemaker potential. The Michaelis constant (Km) was also adjusted to fit the experimental results.

$$I_{NaK} = \frac{P_{NaK}}{1 + (Km_{Nai}/[Na^+]_i)^{1.36}} \frac{1 - ((V + 50)/250)^2}{1 + (Km_{Ko}/[K^+]_o)}. \tag{2.51}$$

(iii) *Plasmalemmal Ca^{2+} pump current (I_{PMCA})*

The plasmalemmal Ca^{2+} pump was clearly demonstrated in the ICCs by Cho & Daniel (2005) using the double-immunofluorescence labelling technique. However, the kinetic properties of the pump are not yet well understood. For this reason, we employed a general approach for the modelling of Ca^{2+} pumps (Fridlyand *et al.* 2003). The half-activation calcium concentration was set to 8 μM to prevent an excessive Ca^{2+} rise in the cytosolic space of ICCs.

$$I_{PMCA} = \frac{P_{PMCA}}{1 + (Km_{Cai}/[Ca^{2+}]_i)^2}. \tag{2.52}$$

(*f*) *IP_3 receptor channel and SR Ca^{2+} dynamics*

(i) *SR Ca^{2+} pump current (I_{up})*

The Ca^{2+} handling by the SR Ca^{2+} pump has been suggested to play a key role in the regulation of Ca^{2+}-dependent pacemaker currents, which were proposed to make a pacemaker depolarization (Hirst *et al.* 2002; Goto *et al.* 2004). The I_{up} was calculated according to the model of Hilgemann & Noble (1987). The basic scheme is identical to that of the Kyoto model (Matsuoka *et al.* 2003) with a slight modification to the Km values and conversion factor (tables 6 and 7).

$$\begin{array}{lll} E_2\mathrm{Ca} \xleftrightarrow{Km_{Cao}} E_2 & & (1-y) \\ k_1 \uparrow\downarrow k_2 \quad k_3 \uparrow\downarrow k_4 & & \beta_y \uparrow\downarrow \alpha_y \\ E_1\mathrm{Ca} \xleftrightarrow{Km_{Cai}} E_1 & & y \end{array}$$

$$I_{up} = P_{up}(k_2 p(E_2\mathrm{Ca})(1-y) - k_1 p(E_1\mathrm{Ca})y), \tag{2.53}$$

$$k_1 = 0.01, \tag{2.54}$$

$$k_2 = 1, \tag{2.55}$$

$$k_3 = 1, \tag{2.56}$$

$$k_4 = 0.01, \tag{2.57}$$

Table 6. SR Ca^{2+} dynamics.

I_{up}	P_{up}: conversion factor, 7728 p(X): probability of state X Km_{Cai}: 0.08 mM Km_{Cao}: 0.002 mM y: gate in the reduced two-state model α_y, β_y: forward and backward rate constants, respectively, of y, ms^{-1}
I_{tr}	P_{tr}: conversion factor, 20.5 pA mM^{-1}
I_{leak}	P_{leak}: conversion factor, 0.45 pA mM^{-1}
I_{IP3R}	P_{IP3R}: conversion factor, 217.2 pA mM^{-1} Km_{Cai}: 0.01 μM

Table 7. Initial values.

$[Ca^{2+}]_i$	cytosolic Ca^{2+} concentration, 38 nM
$[Ca^{2+}]_{rel}$	Ca^{2+} concentration in the release pool of SR, 4.6 mM
$[Ca^{2+}]_{up}$	Ca^{2+} concentration in the uptake pool of SR, 13.1 mM
$[IP_3]$	IP_3 concentration, 0.268 μM
$[PIP_2]$	PIP_2 concentration, 2.66 μM
$[IP_4]$	IP_4 concentration, 0.0067 μM
$[PI_{total}]$	total inositol phosphates concentration, 3.3 μM
$[K^+]_i$	intracellular K^+ concentration, 140 mM
$[K^+]_o$	extracellular K^+ concentration, 5.4 mM
$[Na^+]_i$	intracellular Na^+ concentration, 5.4 mM
$[Na^+]_o$	extracellular Na^+ concentration, 140 mM

$$p(E_1\mathrm{Ca}) = \frac{1}{1 + Km_{\mathrm{Cai}}/[\mathrm{Ca}^{2+}]_{\mathrm{up}}}, \tag{2.58}$$

$$p(E_2\mathrm{Ca}) = \frac{1}{1 + Km_{\mathrm{Cao}}/[\mathrm{Ca}^{2+}]_{\mathrm{i}}}, \tag{2.59}$$

$$p(E_1) = \frac{1}{1 + [\mathrm{Ca}^{2+}]_{\mathrm{up}}/Km_{\mathrm{Cai}}}, \tag{2.60}$$

$$p(E_2) = \frac{1}{1 + [\mathrm{Ca}^{2+}]_{\mathrm{i}}/Km_{\mathrm{Cao}}}, \tag{2.61}$$

$$\alpha_y = k_2 p(E_2\mathrm{Ca}) + k_4 p(E_2), \tag{2.62}$$

$$\beta_y = k_1 p(E_1\mathrm{Ca}) + k_3 p(E_1). \tag{2.63}$$

(ii) *Ca^{2+} transfer from the SR uptake site to the release site (I_{tr})*

In the cardiac myocyte modelling, the SR Ca^{2+} pool was divided into the uptake and release sites to describe the underlying basis for the mechanical restitution and force–frequency relationship (Luo & Rudy 1994; Matsuoka *et al.* 2003). There is also evidence that a force–frequency relationship exists in the gastric smooth muscle cells, a similar cell type to ICC (Fukuta *et al.* 2002). Therefore, we separated the SR Ca^{2+} pool of ICC into two different regions. The Ca^{2+} transfer is suggested to move Ca^{2+} from the uptake site to the release site of the SR to provide Ca^{2+} for the next release. We used the scheme identical to that of the Kyoto model and adjusted the conversion or amplitude factor (P_{tr}) to fit the time course of the autonomous inward current (see figure 3) representing the cytosolic Ca^{2+} transient.

$$I_{tr} = P_{tr}([Ca^{2+}]_{up} - [Ca^{2+}]_{rel}). \tag{2.64}$$

(iii) *Ca^{2+} leak from the SR (I_{leak})*

The I_{leak} was also taken from a scheme identical to that of the Kyoto model, and the conversion factor (P_{leak}) was adjusted to fit the time course of the cytosolic Ca^{2+} transient.

$$I_{leak} = P_{leak}([Ca^{2+}]_{up} - [Ca^{2+}]_{i}). \tag{2.65}$$

(iv) *IP_3-mediated Ca^{2+} release from the SR (I_{IP3R})*

The IP_3-mediated Ca^{2+} release has been suggested to mediate the generation of pacemaker potential via the activation of a Ca^{2+}-dependent inward current (Ward *et al.* 2000; Malysz *et al.* 2001; Goto *et al.* 2004). There is an increasing body of evidence that the I_{IP3R} in the SR is dependent on both the Ca^{2+} and IP_3 concentrations (Bezprozvanny *et al.* 1991; Iino *et al.* 1993; Marchant & Taylor 1997; Taylor & Laude 2002). We employed the model of Marchant & Taylor (1997), which describes the opening of IP_3 receptors by sequential binding of IP_3 and Ca^{2+}. In their scheme, the binding of IP_3 rapidly changes the conformation of the receptor to expose a Ca^{2+}-binding site; Ca^{2+} then binds to this newly exposed site, and the channel opens allowing Ca^{2+} to pass through. They proposed that three or four subunits of the IP_3 receptor must bind IP_3 before the channel opens and releases Ca^{2+} into the cytosol. We added another term, Ca^{2+} concentration at the release site of the SR ($[Ca^{2+}]_{rel}$), to allow the rate of Ca^{2+} release to be dependent on the fluctuation of the SR Ca^{2+} pool (see equation (2.67)). All the rate constants were modified to reproduce the I_{AI}.

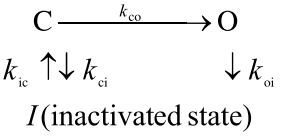

$$I_{IP3R} = P_{IP3R}([Ca^{2+}]_{rel} - [Ca^{2+}]_{i})p_o, \tag{2.66}$$

$$k_{ic} = 0.0025([IP_3]/0.001)^3[Ca^{2+}]_{rel}, \tag{2.67}$$

$$k_{ci} = 0.000849, \tag{2.68}$$

$$k_{co} = 0.147([Ca^{2+}]_i/0.000057)^3, \tag{2.69}$$

$$k_{oi} = 0.02. \tag{2.70}$$

(v) *Ca^{2+} concentration in the SR*

The Ca^{2+} concentrations of the SR uptake and release sites were calculated using the following equations:

$$d[Ca^{2+}]_{up}/dt = (I_{up} - I_{tr} - I_{leak})/(z_{Ca} V_{up} F), \tag{2.71}$$

$$d[Ca^{2+}]_{rel}/dt = (I_{tr} - I_{IP3R})/(z_{Ca} V_{rel} F). \tag{2.72}$$

(*g*) *IP_3 metabolism*

The IP_3 plays a central role in mobilizing Ca^{2+} in eukaryotic cells (Berridge & Irvine 1989; Rana & Hokin 1990). The binding of hormone to the receptors on a cell surface activates the phospholipase C (PLC), which subsequently hydrolyses PIP_2 in the plasma membrane into the IP_3 and diacylglycerol. The IP_3 finally opens a channel on the SR to release the stored Ca^{2+} into the cytosolic space (IP_3-mediated Ca^{2+} release) and IP_3 is then recycled to the plasma membrane after its degradation to the inactive forms. There is an increasing body of evidence that IP_3 formation is also dependent on the membrane depolarization (Vergara *et al.* 1985; Best & Bolton 1986; Wang *et al.* 1995; Ganitkevich & Isenberg 1996; Goto *et al.* 2004). We created a kinetic scheme to reproduce the depolarization-evoked rise of IP_3-mediated Ca^{2+} release in the ICCs from mouse small intestine (Goto *et al.* 2004). The following scheme simplifies the metabolic pathways of inositol phosphates (PIP_2, IP_3, IP_4 and other metabolites):

$$\begin{array}{ccc} PIP_2 & \underset{k_{ba}}{\overset{k_{ab}}{\rightleftarrows}} & IP_3 \\ k_{ca} \uparrow & & \downarrow k_{bc} \\ \multicolumn{3}{c}{IP_4 \text{ (Inactive metabolites)}} \end{array}$$

The time-dependent changes of inositol phosphates can be described by the following equations:

$$d[IP_3]/dt = k_{ab}[PIP_2] - (k_{ba} + k_{bc})[IP_3], \tag{2.73}$$

$$d[PIP_2]/dt = k_{ba}[IP_3] + k_{ca}[IP_4] - k_{ab}[PIP_2], \tag{2.74}$$

$$d[IP_4]/dt = k_{bc}[IP_3] - k_{ca}[IP_4]. \tag{2.75}$$

The total amount of available inositol phosphates was assumed to have a constant value (3.3 μM) during a normal pacemaker activity. The basal level of $[IP_3]$ (less than 50 nM) calculated from our simulation was in a range similar to the value (10 ± 3 nM) obtained by Wang *et al.* (1995).

$$[PI_{total}] = [PIP_2] + [IP_3] + [IP_4]. \tag{2.76}$$

The rate constants of IP_3 production were set to be voltage- and Ca^{2+}-dependent (Vergara *et al.* 1985; Best & Bolton 1986; Biden & Wollheim 1986; Takazawa *et al.* 1990; Wang *et al.* 1995; Ganitkevich & Isenberg 1996; Goto *et al.* 2004). The voltage dependence was given to the forward and backward rate constants to reproduce the voltage-dependent activation of the autonomous inward currents obtained by Goto *et al.* (2004). The forward rate constant was set to increase exponentially as the membrane potential goes into the positive direction, while the backward rate constant was set to decrease exponentially. The Ca^{2+} dependence was also given to the forward rate constant of IP_3 production. Since the Hill function has been used to describe the Ca^{2+} dependence on the IP_3 production (Biden & Wollheim 1986; Takazawa *et al.* 1990; Wang *et al.* 1995; Allen *et al.* 1997), the half-activation by Ca^{2+} (Km_{Cai}) was taken to model the IP_3 production. Km_{Cai} was set to 10 nM, which is close to the basal level of $[IP_3]$ obtained by Wang *et al.* (1995). As for the remaining part of IP_3 metabolic pathways, we set the rate constants empirically to fit the shape of experimentally obtained pacemaker potentials.

$$k_{ab} = 0.2 \exp((V + 48.5)/18.1) \frac{[Ca^{2+}]_i}{[Ca^{2+}]_i + Km_{Cai}}, \tag{2.77}$$

$$k_{ba} = 0.5 \exp((V + 100)/(-28.5)), \tag{2.78}$$

$$k_{bc} = 0.004, \tag{2.79}$$

$$k_{ca} = 0.0035 \exp((V + 100)/(-25.5)). \tag{2.80}$$

3. Results

(*a*) *Reconstruction of pacemaker activity in the mouse ICCs*

We simulated the electrical activity of ICCs from mouse small intestine with the integration of various cellular events as described in §2. As a result, spontaneous and regularly firing APs (pacemaker potential) were successfully reproduced (figure 1). The resting and overshoot potentials were around −78 and +1.2 mV, respectively. The duration of depolarizations was around 639 ms as measured at 50% repolarization. The frequency of pacemaker potentials was around 20 min^{-1}. Compared with the experimental recordings by Goto *et al.* (2004), the frequency is higher in our model cell (20 versus 16.2 min^{-1}, the model simulation versus the experimental recording, respectively) and the duration (639 versus 489.1 ms) is also longer in the model cell. The repetitive firing of APs was very stable throughout the simulation experiment, which exceeded the equivalent of 10 min on a cellular time-scale.

A single pacemaker potential from the mouse ICCs was compared with that from the model simulation (figure 2). The shape of the pacemaker potential is apparently similar between the two recordings (figure 2, *left panel*).

Both the recordings show a low resting potential, abrupt depolarization and repolarization, and a long plateau characteristic of ICCs (Dickens *et al.* 2000). The rising phase of the spontaneous depolarization was also compared between

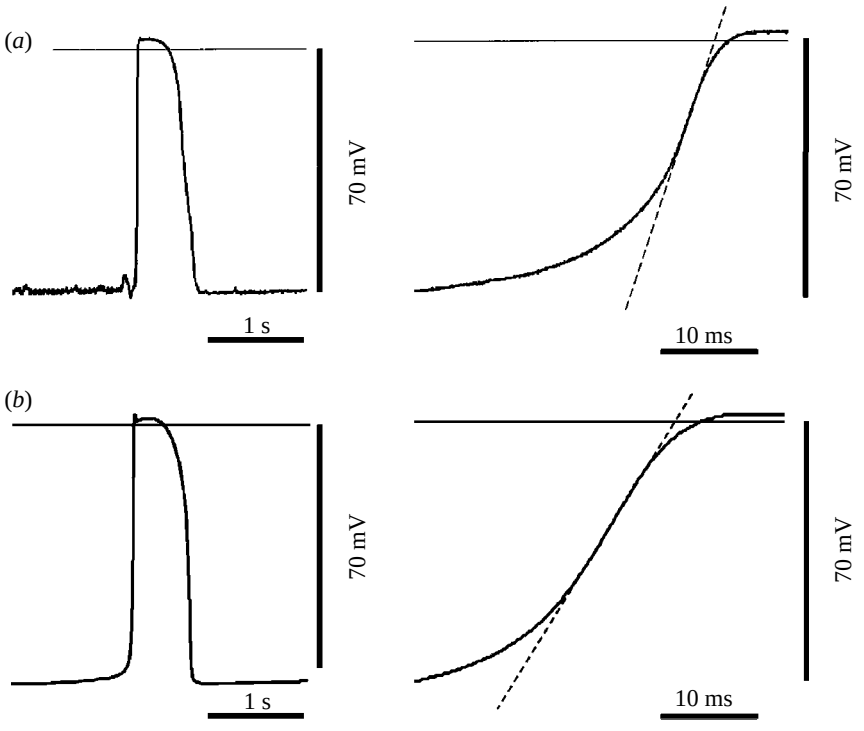

Figure 2. Comparison of the pacemaker potentials in mouse ICCs with those by model simulation. (*a*) A representative trace of a pacemaker potential (*left panel*) and its expanded view (*right panel*), which is recorded from a perforated patch of mouse ICC. The straight horizontal line superimposed on the upper part of the pacemaker potential indicates the zero potential level. The interrupted line superimposed on the expanded trace of the pacemaker potential indicates the maximum rate of rise of the spontaneous depolarization, which was $7.1\ \mathrm{V\,s^{-1}}$ at around -20.8 mV. Reproduced with permission from Goto *et al.* (2004). (*b*) Representative recordings produced by the model simulation. The maximum rise of the spontaneous depolarization was $4.32\ \mathrm{V\,s^{-1}}$ at around -20 mV.

the two recordings in an expanded view (figure 2, *right panel*). The maximum rate of rise is $7.1\ \mathrm{V\,s^{-1}}$ in the experimental recording, while it is $4.32\ \mathrm{V\,s^{-1}}$ in the model simulation. Goto *et al.* (2004) reported other cell groups with a different range of the maximum rate of rise ($3.6 \pm 0.7\ \mathrm{V\,s^{-1}}$ at around -22.2 mV, $n=5$) in the same study. The duration at 50% repolarization was also different for the recording in figure 2 (489.1 ± 32.8 versus 269.5 ± 29.7 ms, $n=5$).

(*b*) *Activation of the I_{AI} by depolarization*

The different value of the maximum rate of rise among the cells indicates that the amplitude of the pacemaker inward current is also variable. Figure 3*a* shows the activation of inward currents in a mouse ICC by depolarization with a conventional voltage-clamp protocol. The holding potential was -80 mV. As a 30 mV depolarization with a duration of 200 ms was applied, a large inward current was evoked after a delay of approximately 20 ms. This large inward current was also evoked with smaller amplitude by larger depolarizations. Interestingly, this inward current showed an autonomous time course lasting

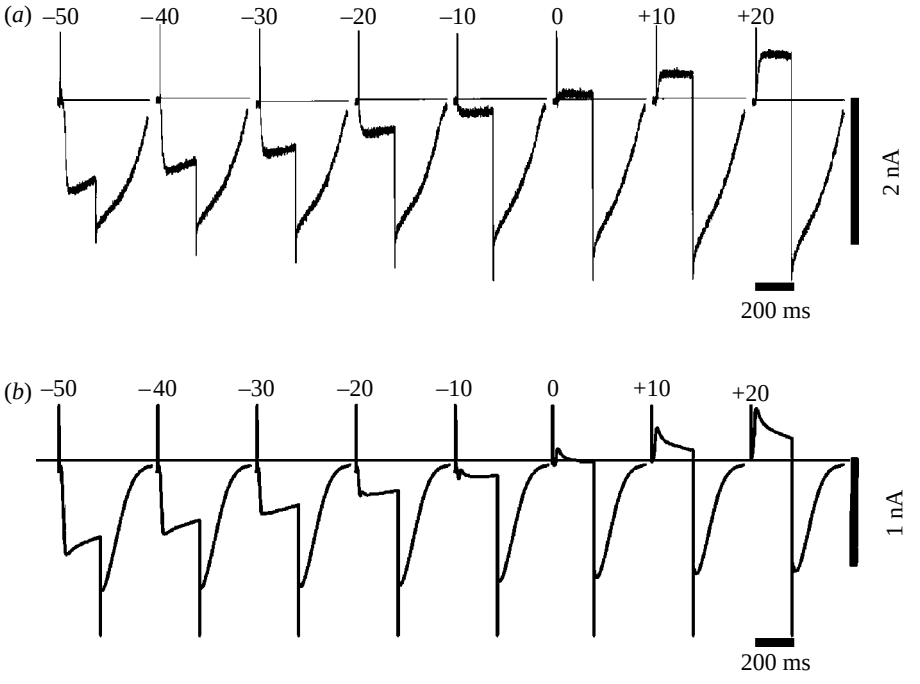

Figure 3. Comparison of the depolarization-induced inward currents (I_{AI}) in voltage-clamped ICCs with those produced by the model simulation. (*a*) Representative current traces in response to test pulses of 200 ms in duration to the potentials indicated above each trace. The holding potential was −80 mV. The horizontal lines indicate the zero current level. Reproduced with permission from Goto *et al.* (2004). (*b*) Representative current traces produced by the model simulation. Note that the current scale along the *y*-axis is different from that in (*a*).

about 500 ms, irrespective of the duration of the depolarizing pulse. The delay in the development of inward current was shortened with a larger depolarization. The time course of the inward current after repolarization to the holding potential was also not changed. Based on these characteristic features, Goto *et al.* (2004) called this inward current the autonomous inward current (I_{AI}). Figure 3*b* shows the recordings made by the model simulation. The model simulation also shows similar inward currents in response to a series of membrane depolarizations. The time course of current relaxation was found to differ between the experimental and simulation recordings. The current size also differed between the two, with smaller amplitude in the simulation recording. The latter observation indicates that the difference in the values for the maximum rate of rise (see figure 2) between two recordings is derived from the different size of the I_{AI}.

(*c*) *Changes in cellular parameters during the occurrence of a pacemaker potential*

Figure 4 shows the time-dependent changes in cellular parameters such as membrane currents, $[Ca^{2+}]_i$, $[IP_3]$, $[Ca^{2+}]_{rel}$ and availability of the IP_3R channel ($P_{o,IP3R}$). The data demonstrate that the major conductance causing

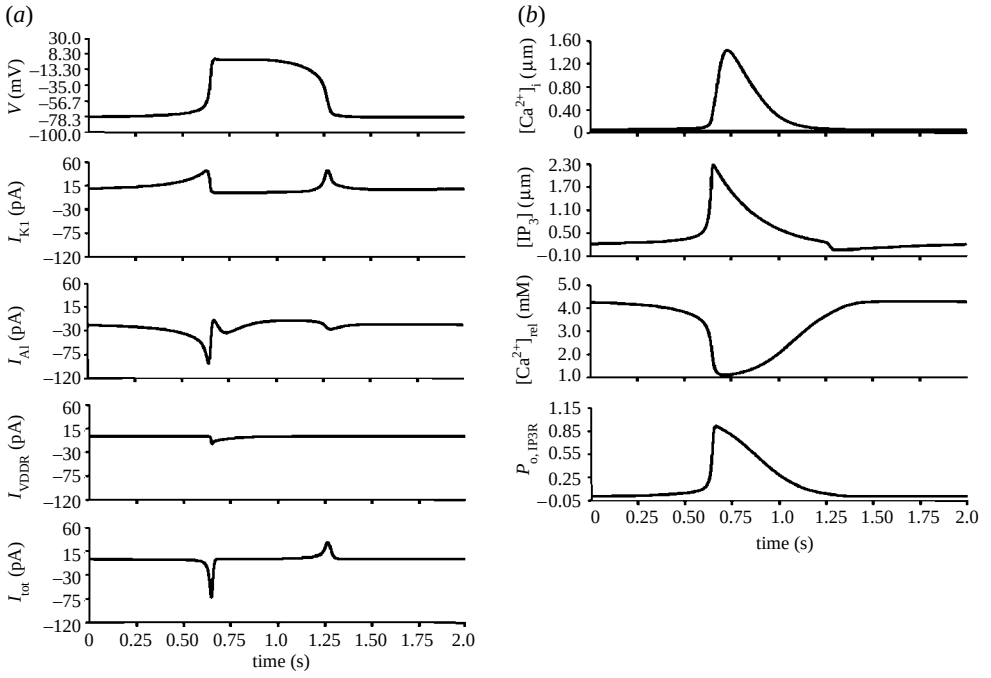

Figure 4. Time-dependent changes in cellular parameters during the period of pacemaker potential occurrence produced by the simulation. (*a*) The individual current components were compared with that of the accompanying pacemaker potential along the time axis. All the individual current components have the same current scale in the figure. (*b*) Time-dependent changes in $[Ca^{2+}]_i$, $[IP_3]$, $[Ca^{2+}]_{rel}$, and the availability of IP_3R ($P_{o,IP3R}$). All the traces have the same time-scale as the pacemaker potential in (*a*).

a pacemaker depolarization in ICCs is I_{AI} and that the conductance causing the repolarization is I_{K1} (figure 4*a*). The close relationship among the time courses of membrane potential, $[IP_3]$, $[Ca^{2+}]_i$ and $P_{o,IP3R}$ favours the hypothesis that cyclic changes in IP_3 and $Ca^{2+}{}_i$ might play a central role in the pacemaker mechanism (Van Helden *et al.* 2000; Goto *et al.* 2004).

4. Discussion and conclusions

Our model faithfully reproduces the pacemaker activity of the intestinal ICCs. Spontaneous and repetitive firing of APs continues as long as the simulation is running. The initial triggering event is thought to begin with the Ca^{2+} leak from the SR and the DHP-resistant pathway (I_{VDDR}) (Kim *et al.* 2002). In fact, the removal of the Ca^{2+} leak from the SR and plasma membrane abolished the spontaneous activity of the model (data not shown). A local rise in Ca^{2+} concentration near the SR activates the IP_3-mediated Ca^{2+} release (Berridge 1990; Bezprozvanny *et al.* 1991; Jaffe 1991; Iino *et al.* 1993; Marchant & Taylor 1997; Taylor & Laude 2002). In addition, cytosolic Ca^{2+} concentration enhances the IP_3 production by the activation of IP_3 3-kinase (Biden & Wollheim 1986; Takazawa *et al.* 1990; Wang *et al.* 1995). Taken together, Ca^{2+} release and IP_3 production work in a cooperative manner and make a positive feedback to

increase $[Ca^{2+}]_i$. An increase in the Ca^{2+} concentration in the subsarcolemmal region to a threshold value activates Ca^{2+}-activated channels, which depolarize the cell membrane (Hirst *et al.* 2002; Goto *et al.* 2004). The membrane depolarization has an additional effect of enhancing IP_3 production (Vergara *et al.* 1985; Best & Bolton 1986; Wang *et al.* 1995; Ganitkevich & Isenberg 1996; Goto *et al.* 2004). A prolonged increase of IP_3 production by membrane depolarization creates the plateau phase of the pacemaker potential. The depletion of the Ca^{2+} pool and the gradual decrease of the available IP_3 pool are thought to terminate the plateau phase. A repolarization to the threshold level finally activates the inward rectifier K^+ channel, which restores the membrane potential to the resting level.

Although our model reproduces the pacemaker activity faithfully, it is unclear whether the parameter values used here appropriately reflect the real dynamics and homeostasis of a cell. There are so many interactions between parameter values that it is nearly impossible to obtain a single solution set that fits the experimental results. Each component of modelling should be validated by carefully designed experiments. For example, the effect of $[Ca^{2+}]_{rel}$ on the recovery of IP_3 receptor channel from the inactivated state is based on many cardiac models in which there is more direct evidence for SR Ca^{2+}-load dependence on ryanodine release channels (Matsuda & Noma 1984). It should be validated experimentally. Even though our model needs additional validation and improvement in the near future, it is thought that the model has a value in that it provides a system to test the accumulated results and hypotheses on the pacemaker activity of ICCs.

Editors' note

Please see also related communications in this focussed issue by Steinberg *et al.* (2006) and Terashima *et al.* (2006).

This work was supported by funds from the Advanced Backbone IT Technology Development Project of the Ministry of Information and Communication (IMT-2000-C3-5; IMT-2000-C3-3) and the Leading Project for Biosimulation from the Ministry of Education, Culture, Sports, Science and Technology of Japan.

References

Allen, V., Swigart, P., Cheung, R., Cockcroft, S. & Katan, M. 1997 Regulation of inositol lipid-specific phospholipase Cδ by changes in Ca^{2+} ion concentrations. *Biochem. J.* **327**, 545–552.

Berridge, M. J. 1990 Calcium oscillations. *J. Biol. Chem.* **265**, 9583–9586.

Berridge, M. J. & Irvine, R. F. 1989 Inositol phosphates and cell signalling. *Nature* **341**, 197–205. (doi:10.1038/341197a0)

Best, L. & Bolton, T. B. 1986 Depolarisation of guinea-pig visceral smooth muscle causes hydrolysis of inositol phospholipids. *Naunyn Schmiedebergs Arch. Pharmacol.* **333**, 78–82. (doi:10.1007/BF00569664)

Bezprozvanny, I., Watras, J. & Ehrlich, B. E. 1991 Bell-shaped calcium-response curves of Ins(1,4,5)P3- and calcium-gated channels from endoplasmic reticulum of cerebellum. *Nature* **351**, 751–754. (doi:10.1038/351751a0)

Biden, T. J. & Wollheim, C. B. 1986 Ca^{2+} regulates the inositol tris/tetrakisphosphate pathway in intact and broken preparations of insulin-secreting RINm5F cells. *J. Biol. Chem.* **261**, 11 931–11 934.

Cho, W. J. & Daniel, E. E. 2005 Proteins of interstitial cells of Cajal and intestinal smooth muscle, colocalized with caveolin-1. *Am. J. Physiol. Gastrointest. Liver Physiol.* **288**, G571–G585. (doi:10.1152/ajpgi.00222.2004)

Dickens, E. J., Hirst, G. D. S. & Tomita, T. 1999 Identification of rhythmically active cells in guinea-pig stomach. *J. Physiol.* **514**, 515–531. (doi:10.1111/j.1469-7793.1999.515ae.x)

Dickens, E. J., Edwards, F. R. & Hirst, G. D. 2000 Vagal inhibition in the antral region of guinea pig stomach. *Am. J. Physiol. Gastrointest. Liver Physiol.* **279**, G388–G399.

Edwards, F. R. & Hirst, G. D. S. 2003 Mathematical description of regenerative potentials recorded from circular smooth muscle of guinea pig antrum. *Am. J. Physiol. Gastrointest. Liver Physiol.* **285**, G661–G670.

Edwards, F. R. & Hirst, G. D. S. 2005 An electrical description of the generation of slow waves in the antrum of the guinea-pig. *J. Physiol.* **564**, 214–232. (doi:10.1113/jphysiol.2004.077123)

Fridlyand, L. E., Tamarina, N. & Philipson, L. H. 2003 Modeling of Ca^{2+} flux in pancreatic beta-cells: role of the plasma membrane and intracellular stores. *Am. J. Physiol. Endocrinol. Metab.* **285**, E138–E154.

Fukuta, H., Kito, Y. & Suzuki, H. 2002 Spontaneous electrical activity and associated changes in calcium concentration in guinea-pig gastric smooth muscle. *J. Physiol.* **540**, 249–260. (doi:10.1113/jphysiol.2001.013306)

Ganitkevich, V. Y. & Isenberg, G. 1996 Effect of membrane potential on the initiation of acetylcholine-induced Ca^{2+} transients in isolated guinea pig coronary myocytes. *Circ. Res.* **78**, 717–723.

Goto, K., Matsuoka, S. & Noma, A. 2004 Two types of spontaneous depolarizations in the interstitial cells freshly prepared from the murine small intestine. *J. Physiol.* **559**, 411–422. (doi:10.1113/jphysiol.2004.063875)

Hilgemann, D. W. & Noble, D. 1987 Excitation–contraction coupling and extracellular calcium transients in rabbit atrium: reconstruction of basic cellular mechanisms. *Proc. R. Soc. B* **230**, 163–205.

Hirst, G. D. S., Bramich, N. J., Teramoto, N., Suzuki, H. & Edwards, F. R. 2002 Regenerative component of slow waves in the guinea-pig gastric antrum involves a delayed increase in $[Ca^{2+}]_i$ and Cl^- channels. *J. Physiol.* **540**, 907–919. (doi:10.1113/jphysiol.2001.014803)

Iino, M., Yamazawa, T., Miyashita, Y., Endo, M. & Kasai, H. 1993 Critical intracellular Ca^{2+} concentration for all-or-none Ca^{2+} spiking in single smooth muscle cells. *EMBO J.* **12**, 5287–5291.

Jaffe, L. F. 1991 The path of calcium in cytosolic calcium oscillations: a unifying hypothesis. *Proc. Natl Acad. Sci. USA* **88**, 9883–9887.

Kim, Y. C., Koh, S. D. & Sanders, K. M. 2002 Voltage-dependent inward currents of interstitial cells of Cajal from murine colon and small intestine. *J. Physiol.* **541**, 797–810. (doi:10.1113/jphysiol.2002.018796)

Koh, S. D., Sanders, K. M. & Ward, S. M. 1998 Spontaneous electrical rhythmicity in cultured interstitial cells of Cajal from the murine small intestine. *J. Physiol.* **513**, 203–213. (doi:10.1111/j.1469-7793.1998.203by.x)

Koh, S. D., Jun, J. Y., Kim, T. W. & Sanders, K. M. 2002 A Ca^{2+}-inhibited non-selective cation conductance contributes to pacemaker currents in mouse interstitial cell of Cajal. *J. Physiol.* **540**, 803–814. (doi:10.1113/jphysiol.2001.014639)

Luo, C. H. & Rudy, Y. 1994 A dynamic model of the cardiac ventricular action potential. I. Simulations of ionic currents and concentration changes. *Circ. Res.* **74**, 1071–1096.

Mackenzie, L., Bootman, M. D., Berridge, M. J. & Lipp, P. 2001 Predetermined recruitment of calcium release sites underlies excitation–contraction coupling in rat atrial myocytes. *J. Physiol.* **530**, 417–429. (doi:10.1111/j.1469-7793.2001.0417k.x)

Malysz, J., Donnelly, G. & Huizinga, J. D. 2001 Regulation of slow wave frequency by IP_3-sensitive calcium release in the murine small intestine. *Am. J. Physiol. Gastrointest. Liver Physiol.* **280**, G439–G448.

Marchant, J. S. & Taylor, C. W. 1997 Cooperative activation of IP_3 receptors by sequential binding of IP_3 and Ca^{2+} safeguards against spontaneous activity. *Curr. Biol.* **7**, 510–508. (doi:10.1016/S0960-9822(06)00222-3)

Matsuda, H. & Noma, A. 1984 Isolation of calcium current and its sensitivity to monovalent cations in dialysed ventricular cells of guinea-pig. *J. Physiol.* **357**, 553–573.

Matsuoka, S., Sarai, N., Kuratomi, S., Ono, K. & Noma, A. 2003 Role of individual ionic current systems in ventricular cells hypothesized by a model study. *Jpn. J. Physiol.* **53**, 105–123. (doi:10.2170/jjphysiol.53.105)

Miftakhov, R. N., Abdusheva, G. R. & Christensen, J. 1999 Numerical simulation of motility patterns of the small bowel. 1. Formulation of a mathematical model. *J. Theor. Biol.* **197**, 89–112. (doi:10.1006/jtbi.1998.0859)

Powell, T., Noma, A., Shioya, T. & Kozlowski, R. Z. 1993 Turnover rate of the cardiac Na^+–Ca^{2+} exchanger in guinea-pig ventricular myocytes. *J. Physiol.* **472**, 45–53.

Rana, R. S. & Hokin, L. E. 1990 Role of phosphoinositides in transmembrane signaling. *Physiol. Rev.* **70**, 115–164.

Sakai, R., Hagiwara, N., Matsuda, N., Kassanuki, H. & Hosoda, S. 1996 Sodium–potassium pump current in rabbit sino-atrial node cells. *J. Physiol.* **490**, 51–62.

Steinberg, B. E., Glass, L., Shrier, A. & Bub, G. 2006 The role of heterogeneities and intercellular coupling in wave propagation in cardiac tissue. *Phil. Trans. R. Soc. A* **364**, 1299–1311. (doi:10.1098/rsta.2006.1771)

Takazawa, K., Lemos, M., Delvaux, A., Lejeune, C., Dumont, J. E. & Erneux, C. 1990 Rat brain inositol 1,4,5-trisphosphate 3-kinase. Ca^{2+}-sensitivity, purification and antibody production. *Biochem. J.* **268**, 213–217.

Taylor, C. W. & Laude, A. J. 2002 IP_3 receptors and their regulation by calmodulin and cytosolic Ca^{2+}. *Cell Calcium* **32**, 321–334. (doi:10.1016/S0143416002001859)

Terashima, K., Takeuchi, A., Sarai, N., Matsuoka, S., Shim, E. B., Leem, C. H. & Noma, A. 2006 Modelling Cl^- homeostasis and volume regulation of the cardiac cell. *Phil. Trans. R. Soc. A* **364**, 1245–1265. (doi:10.1098/rsta.2006.1767)

Tomita, T. 1981 Electrical activity (spikes and slow waves) in gastrointestinal smooth muscles. In *Smooth muscle: an assessment of current knowledge* (ed. E. Bulbring, A. F. Brading, A. W. Jones & T. Tomita), pp. 127–156. London: Edward Arnold.

Van Helden, D. F., Imtiaz, M. S., Nurgaliyeva, K., von der Weid, P.-Y. & Dosen, P. J. 2000 Role of calcium stores and membrane voltage in the generation of slow wave action potentials in guinea-pig gastric pylorus. *J. Physiol.* **524**, 245–265. (doi:10.1111/j.1469-7793.2000.00245.x)

Vergara, J., Tsien, R. Y. & Delay, M. 1985 Inositol 1,4,5-trisphosphate: a possible chemical link in excitation–contraction coupling in muscle. *Proc. Natl Acad. Sci. USA* **82**, 6352–6356.

Wang, S. S., Alousi, A. A. & Thompson, S. H. 1995 The lifetime of inositol 1,4,5-trisphosphate in single cells. *J. Gen. Physiol.* **105**, 149–171. (doi:10.1085/jgp.105.1.149)

Ward, S. M., Ordog, T., Koh, S. D., Baker, S. A., Jun, J. Y., Amberg, G., Monaghan, K. & Sanders, K. M. 2000 Pacemaking in interstitial cells of Cajal depends upon calcium handling by endoplasmic reticulum and mitochondria. *J. Physiol.* **525**, 355–361. (doi:10.1111/j.1469-7793.2000.t01-1-00355.x)